Proceedings of the 4th International Conference on Modern Medicine and Global Health
DOI: 10.54254/2753-8818/2026.LA30799

A Mini-Review of Perovskite Solar Cells before and after Graphene Implementation

Haofeng Xiang

Australian International School, Singapore, Singapore
haofengxiang11808@gmail.com

Abstract. Perovskite solar cells (PSCs) have become well-known innovative devices for their high power conversion efficiency with low manufacturing cost compared to others. However, several drawbacks illustrate their great potential of improving more. In recent years, graphene and its derivatives have been introduced into PSCs to improve charge transport, defect passivation, and environmental durability. This article compares the performance of perovskite devices before and after the incorporation of graphene; analyzes its role in the charge transport layer, perovskite absorber layer, and electrodes; and discusses the present challenges and future potential of using graphene-based perovskite photovoltaic systems.

Keywords: Perovskite solar cells, Graphene, Charge transport, Stability, Transparent electrodes

1. Introduction

Over the past few years, perovskite solar cells (PSCs) have developed from experimental devices to efficient products in reality that can now compete with silicon photovoltaics. Their fast rise can be attributed to a combination of favorable material properties—strong absorption across the visible spectrum, long carrier transport distances, and a certain tolerance toward point defects—together with solution-based fabrication routes that consume little energy [1]. These strengths mean PSCs could, in principle, be produced inexpensively at scale. Despite this promise, the perovskite absorber is far from stable: water and oxygen trigger decomposition pathways, UV exposure accelerates chemical changes at critical interfaces, and heating may alter crystal phases or activate ion migration [2,3]. Compared to that, the commonly employed transparent electrodes (for example, ITO and FTO) are stiff, costly, and breakable, which makes it almost impossible to retain their performance in flexible or wearable forms. Hence, stability is the main factor that separates the mass production of PSCs from the market, not just efficiency [4].

Recent research has explored how graphene can improve electron and hole transport layers, alter the perovskite crystal structure, and replace traditional transparent electrodes. This mini review superficially analyzes how graphene affects charge transfer, structural stability, and mechanical flexibility in PSCs and explores the challenges that still exist in future applications.

© 2026 The Authors. This is an open access article distributed under the terms of the Creative Commons Attribution License 4.0 (https://creativecommons.org/licenses/by/4.0/).

DOI: 10.54254/2753-8818/2026.LA30799

2. Preparation method

2.1. Device architectures: n-i-p/p-i-n

In planar perovskite solar cells, researchers usually adopt one of two structural configurations: the n–i–p and the p–i–n stack. The n–i–p layout, which appeared earlier in the development of PSCs, begins with a transparent conducting oxide layer such as fluorine-doped tin oxide (FTO) or indium tin oxide (ITO). On top of this, an electron transport layer is deposited, most commonly compact or mesoporous titanium dioxide (TiO_2) or, in low-temperature systems, tin dioxide (SnO_2). This is followed by the perovskite absorber, then a hole transport material such as Spiro-OMeTAD or PTAA, and finally a metallic contact layer—usually silver or gold—that completes the device and allows charge collection [1,5,6].

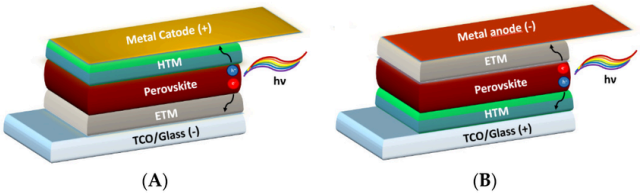


Figure 1. Schematic diagrams of (A) conventional n–i–p (direct) and (B) inverted p–i–n perovskite solar cell structures

By contrast, the p–i–n or "inverted" architecture reverses the order of the charge transport layers. In this case, the transparent conducting oxide is first coated with a hole transport material, which can be a self-assembled monolayer (SAM) like MeO-2PACz or 2PACz, or a polymer such as PEDOT: PSS. The perovskite layer is then formed above it, and the top interface consists of an electron transport layer—often thermally evaporated C_{60} with a thin BCP buffer—before being finished with a metallic electrode made of copper or silver [7-9].

Although both structures rely on the same fundamental working principles, they differ in processing and performance characteristics. The n–i–p design is compatible with high-temperature oxide layers and traditional mesoporous scaffolds, which makes it stable and well-understood, but less suitable for flexible substrates or scalable manufacturing. The p–i–n architecture, on the other hand, allows low-temperature fabrication and produces smoother buried interfaces due to the use of SAMs. Inverted architecture. Recent inverted perovskite cells combine >26% power conversion efficiency with long operational stability, so they are now the default choice for tandems and for large-scale production [10].

2.2. Solution processing

In solution processing, the absorber can be created by dissolving lead halides together with organic or inorganic cations in coordinating solvents and casting the mixture in a single coating step. Film formation in this "all-in-one" route is governed by transient solvent–salt complexes that control supersaturation and intermediate phases. Because humidity perturbs this chemistry, the polarity and volatility of solvents such as DMF or DMSO must be balanced to obtain smooth, compact layers and to limit defect formation that would otherwise harm stability [11].

DOI: 10.54254/2753-8818/2026.LA30799

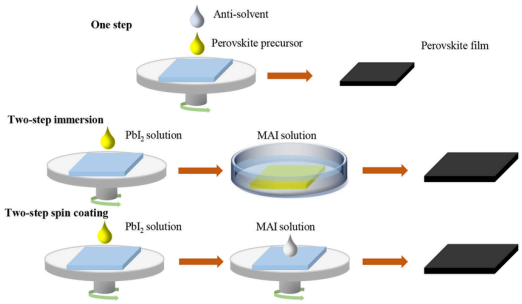


Figure 2. Diagram showing the one-step and two-step methods commonly used for perovskite film preparation

A second strategy separates conversion from deposition. A dense PbI_2 layer is deposited first to guarantee uniform coverage and thickness, and is then transformed into perovskite by exposure to organic halides (for example MAI or FAI) through immersion or a second spin pass. The stepwise reaction slows nucleation and allows more regular grain growth, yielding larger grains, improved morphology, and less disturbance of underlying layers. This control over conversion pathways has enabled high-quality inverted devices with certified efficiencies around 26% [12].

Anti-solvent quenching further refines the crystallization stage. During spinning, a timed drop of a poor solvent such as chlorobenzene or ethyl acetate rapidly extracts the primary solvent, creates supersaturation, and drives uniform nucleation of pinhole-free films. The approach is simple and low-cost, but many of the classic anti-solvents are volatile and toxic, which complicates environmental compliance and factory safety. Current work therefore targets greener substitutes and protocols that preserve the same fast-drying kinetics while fitting meniscus-coating and roll-to-roll lines [13] However, many traditional anti-solvents are toxic and volatile, making them unsuitable for large-scale production. To address this, safer and more environmentally friendly alternatives are being developed for scalable coating and roll-to-roll manufacturing processes.

2.3. Scalable coating & vacuum routes

Since roughly 2013, research has moved from benchtop spin coating toward processes compatible with continuous manufacturing. Meniscus-type coating—slot-die, blade, and spray—offers precise wet-film control, high material utilization, and easy coupling to web handling. Uniformity depends on the flow regime of the wet film, solvent system and drying rate, substrate temperature, web speed, and the design of in-line drying or gas-knives. Reports highlight slot-die as a particularly tractable route because its process window can be mapped through parameters such as coating gap, flow rate, and capillary number, enabling reproducible thickness and coverage at scale. In parallel, vacuum deposition—either sequential or co-evaporative—eliminates liquid solvents altogether, gives tight control over stoichiometry and multilayer stacks, and naturally extends to large-area modules. Although capital costs and throughput optimization remain practical considerations, these vacuum routes pair well with tandem structures and provide solvent-free pathways for high-uniformity production [14, 15].

DOI: 10.54254/2753-8818/2026.LA30799



Figure 3. Evolution of slot-die coating methods and significant milestones from 2013 to the present and onward [16]

Following early proof-of-concept devices, research gradually shifted toward achieving consistent film quality at the module scale. Fully roll-to-roll fabrication of hybrid perovskite modules has now been demonstrated on industrial tools, including routes that replace vacuum-deposited metal electrodes with printed carbon, representing an important step toward low-cost and flexible modules [17].

Control of drying during large-area deposition is another key challenge. Semi-sealed gas-quenching systems have been shown to reduce performance losses in blade-coated perovskite films by stabilizing solvent removal under controlled airflow [18]. At the same time, the application of Landau–Levich scaling laws provides a useful relationship between coating speed, viscosity, and film thickness, helping define process windows for uniform coating [19].

In parallel, vacuum and hybrid approaches have been introduced to replace the anti-solvent dripping methods commonly used in laboratories. Vacuum-driven pre-crystallization techniques allow early solvent removal and more controlled crystal growth, leading to efficient all-perovskite cells. Sequential vacuum evaporation has also produced highly efficient films with well-defined interfaces [20]. A combined solution–vacuum workflow has recently produced 30 cm × 30 cm pinhole-free perovskite sub-modules with a certified efficiency of 21.79%, underscoring its suitability for stable, large-area manufacturing [21].

2.4. Charge-selective contacts engineering

In planar devices, contact layers largely set both efficiency and durability. On the electron-transport side, SnO_2 remains the workhorse because its band alignment, transparency, and low-temperature compatibility are difficult to beat. Mild bulk doping or targeted surface treatments suppress interfacial trap states, which accelerate extraction and extend operational lifetime. Graphene-derived additives are especially effective: embedding graphene quantum dots into SnO_2 smooths the surface, reduces roughness, and improves electron mobility, effects that translate into higher fill factors and power-conversion efficiency [22,23]. These SnO_2–graphene hybrids are therefore viewed as a practical bridge between scalable processing and device stability.

On the hole-transport side, self-assembled monolayers (SAMs) have redefined inverted p-i-n stacks. Ultra-thin, energetically well-aligned SAMs form at low temperature and passivate buried interfaces while ensuring uniform coverage of the transparent electrode. Widely used molecules such as MeO-2PACz and 2PACz build ordered monolayers that curb interfacial recombination; pairing these SAMs with a thin NiO_x interlayer further improves film uniformity and chemical passivation, enabling record fill factors near 84% and device efficiencies around 22% [24,25] aken together, advances in SAM chemistry and the judicious combination of organic monolayers with inorganic interlayers now define the state of the art in hole-selective contact engineering for next-generation perovskite photovoltaics.

DOI: 10.54254/2753-8818/2026.LA30799

2.5. Electrodes and encapsulation

Choosing robust electrodes is pivotal for long-lived perovskite modules. The bottom transparent conductor—usually FTO or ITO—sets the trade-off between optical transmission and sheet resistance, while the top metal contact (often Ag, Cu, or Au) frequently limits lifetime through diffusion and corrosion. A promising remedy is a Cu–Ni alloy electrode formed in situ and clad on both sides with graphene, which acts as an ion-blocking, chemically inert barrier. This hybrid stack markedly enhances operational stability and elevates electrode reliability as a central milestone on the path to durable PSCs [26,27].

Commercial viability also rests on encapsulation that resists moisture, oxygen, UV exposure, and thermal cycling. Current solutions span rigid glass–glass laminates and flexible thin-film barriers; recent designs additionally address lead containment and incorporate stress-relief geometries to mitigate mechanical strain. Epoxy-based sealants tested under standardized outdoor protocols show that well-engineered edge-seals and barrier stacks can satisfy long-term field-stability targets [9,28].

3. Non-graphene-based perovskite solar cells

As a baseline for comparison, this section reviews the physical mechanisms and device performance of perovskite solar cells (PSCs) without graphene modification. These results establish the reference point for evaluating how graphene-based engineering changes transport, recombination, stability, and overall efficiency.

3.1. Working mechanism

Charge transport in PSCs can be described by a coupled drift–diffusion and Poisson model that includes the densities of electrons, holes, ionized donors and acceptors, and mobile ionic defects. These equations represent the motion of both fast electronic carriers and slow-moving ions, whose interaction determines internal field distribution and current response. Drift–diffusion modeling has thus become a key tool for analyzing field screening and hysteresis phenomena, especially when additional continuity equations for positive and negative ions are included to reproduce transient current–voltage behavior [29].

Non-radiative recombination is one of the main loss channels limiting PSC efficiency. It primarily originates from undercoordinated Pb^{2+} ions at perovskite–transport layer interfaces, which form deep trap states that reduce the open-circuit voltage and fill factor [30,31]. In inverted cells, non-radiative recombination at the perovskite/C_{60} interface has been identified as a key factor constraining performance [32]. Sub-bandgap defects contribute little to radiative loss but strongly affect non-radiative voltage losses [33]. Passivating interfacial traps using molecular or polymeric interlayers can halve defect densities and improve photoluminescence quantum yield [34].

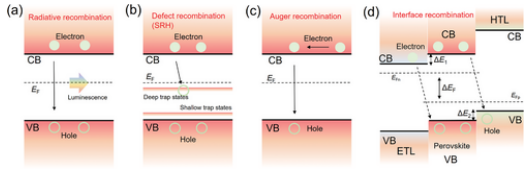


Figure 4. Carrier recombination pathways in solar cells: (a) radiative photon emission; (b) defect-assisted Shockley–Read–Hall via trap states; (c) multiparticle Auger; (d) interface-driven losses from band offsets and interfacial defects [35]

DOI: 10.54254/2753-8818/2026.LA30799

Reducing interface non-radiative recombination is vital for achieving high efficiency. Dual molecular treatments demonstrate synergistic passivation effects: methylphosphonic acid (MPA) forms P–O–Pb covalent bonds that lower defect density, while phenethylammonium iodide (PEAI) introduces a surface dipole to improve electron extraction. This strategy yields p–i–n devices with stabilized efficiencies of 25.5 % and non-radiative voltage losses of only 59 mV [30]. On the buried interface, self-assembled monolayers (SAMs) improve energy alignment and morphology; however, stable anchoring is necessary because polar solvents can desorb weakly bonded SAMs. Covalently bonded SAMs achieve certified efficiencies of 24.6 % and maintain over 98 % of initial performance after 1000 h of damp-heat and 85 °C operation [25].

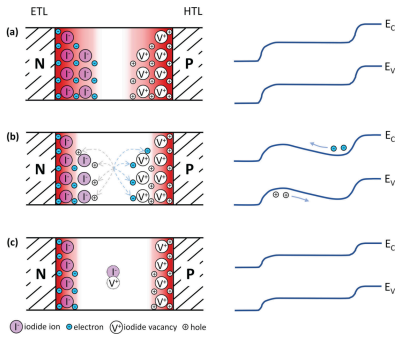


Figure 5. Schematic of ionic redistribution in perovskite solar cells and its impact on band profiles: (a) initial distribution near the ETL/HTL, (b) drift and accumulation of halide vacancies/ions under operation, and (c) partially screened fields after relaxation [36]

Mobile ionic species provide a physical basis for the scan-rate–dependent current–voltage hysteresis seen in many PSCs. Because these ions move slowly compared with electronic carriers, their redistribution lags the voltage sweep, distorting the internal electric field and producing history-dependent I–V curves [37,38]. With extended operation, continued accumulation at interfaces screens the built-in field and can catalyze longer-term degradation pathways [39]. Direct imaging has visualized photo-driven halide migration over distances of hundreds of micrometers, confirming that ion motion is not confined to local grains but can span macroscopic regions of the film [40]. In devices engineered for minimal hysteresis, the density of mobile ions is typically on the order of 10^{15}-10^{17} cm^{-3}, consistent with partial but not negligible field modulation [39].

Wide-bandgap perovskites present an additional challenge: halide phase segregation. Vacancy-assisted migration of halogens promotes separation into iodide-rich and bromide-rich domains, undermining both efficiency and stability [41]. During crystallization, bromide-rich areas often nucleate and solidify earlier, yielding wrinkled topographies and nonuniform morphology [42]. Targeted chemistry can counter these trends. Thiocyanate (SCN^-) and related additives refine nucleation, impede halide motion, and suppress segregation; carefully designed dual-additive systems produce dense, smooth WBG absorbers that have achieved record-level metrics—approximately 22% efficiency with an open-circuit voltage near 1.25 V [43]. Interfacial engineering that limits ion accumulation operates synergistically with these bulk strategies, which consequently reduces hysteresis and delays field-induced degradation [44].

DOI: 10.54254/2753-8818/2026.LA30799

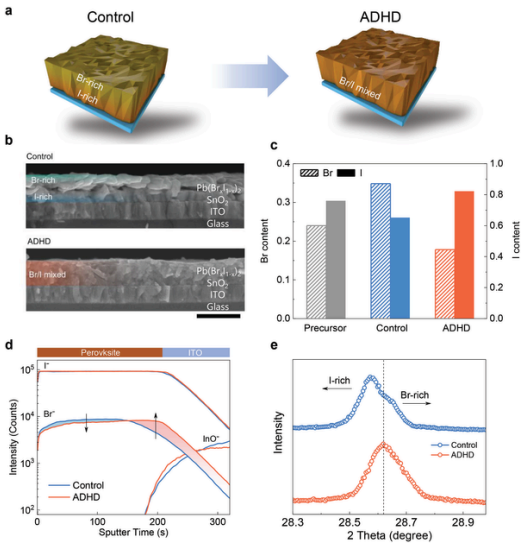


Figure 6. Analysis of the halide composition and phase distribution in control and ADHD perovskite films, including schematic illustration, SEM cross-sections, elemental ratios, depth profiles, and XRD patterns [16]

3.2. Device performance parameters

Steady improvements in absorber quality and interface control have pushed non-graphene perovskite cells close to their theoretical limits. For wide-bandgap devices, open-circuit voltages of about 1.29–1.31 V are now routine, with voltage deficits kept below 0.40 V, and certified efficiencies surpassing 22% [33,45,46]. The present single-junction record is 26.7%, confirmed by NREL [47]. Textured device designs can recover up to ~95% of the Shockley–Queisser current limit without sacrificing fill factor [48], while inverted cells at the 1 cm² level regularly deliver fill factors above 86% [49]. Transport measurements indicate electron mobilities near 45 $cm^2 V^{-1} s^{-1}$ and carrier diffusion lengths reaching ~4 μm, consistent with long-range, low-loss charge transport [50-52]. Encapsulation has also matured: modules subjected to 85 °C/85% RH for 1000 h retain over 90% of their initial output, meeting stringent durability targets for deployment [53,54]. These metrics establish a practical baseline for evaluating any additional gains from graphene integration.

4. Graphene-based PSCs

4.1. Graphene in charge transport layers

4.1.1. Graphene in electron transport layers

Integrating graphene and its derivatives into PSCs helps overcome several limitations in electron transport, interface, and environmental stability. At different locations within the device structure, graphene can serve as a conductive channel and an intermediate for different energy levels to improve the device [2,3].

DOI: 10.54254/2753-8818/2026.LA30799

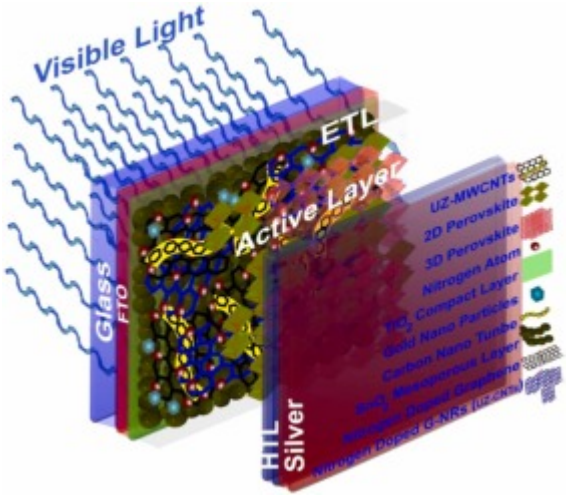


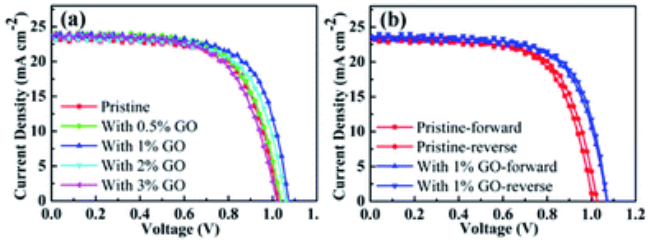
Figure 7. Schematic of a hybrid structure combining TiO_2/SnO_2 with graphene nanoribbons and nanoparticles [4]

Electron-transport layers (ETLs) such as TiO_2 and SnO_2 have mediocre conductivities and surface defects that hinder the extraction of the charges. Introducing reduced graphene oxide (RGO) into ETLs will produce conductive channels and passivate traps, which decrease series resistance and enhance electron mobility, as RGO promotes a smoother flow of electrons within the device stack. This leads to increased photocurrents and a reduced hysteresis effect as compared to pristine ETLs. Traditional hole transport layers (HTLs) absorb moisture easily, leading to a decrease in conductivity. Integrating graphene oxide (GO) sheets can improve HTL film quality and address moisture absorption issues by reducing misalignment between energy levels in hole transport.

Placing graphene at interfaces also plays a role in passivating defects of the different energy levels of different materials and thus reducing energy losses caused by non-radiative recombination. At grain boundaries, graphene quantum dots reduce the number of under-coordinated Pb^{2+} ions [3], improving charge extraction efficiency. This also extends battery life and reduces voltage loss.

4.1.2. Graphene as an additive in the perovskite layer

Graphene derivatives slow down perovskite nucleation, promoting the formation of larger, more uniform grains. This reduces pinholes in the film and minimizes grain boundaries [55].



DOI: 10.54254/2753-8818/2026.LA30799

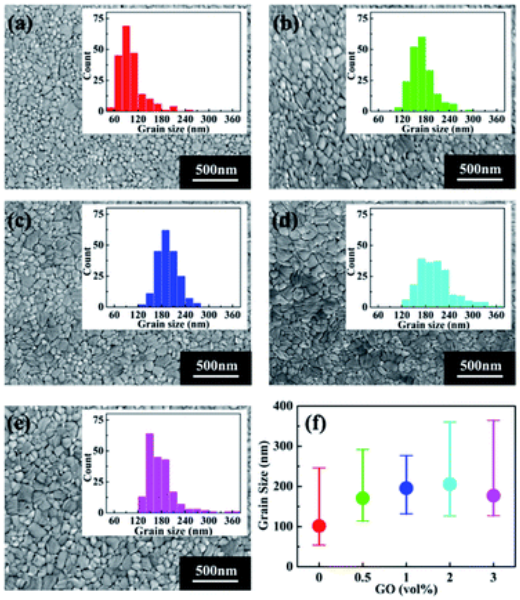


Figure 8. The grain size increases with the graphene oxide (GO) concentration in the precursor solution [55]

Graphene enhances the Jsc and fill factor. It also reduces trap-assisted recombination and prolongs carrier lifetime, thereby achieving higher power conversion efficiency (PCE). Operational stability is also improved, as graphene-doped films demonstrate greater resistance to moisture and light-induced degradation.

4.2. Graphene in transparent electrodes and photomechanical protection

4.2.1. Transparent electrodes

Traditional transparent conductive oxides are brittle and rely on scarce indium resources. Graphene and its derivatives can serve as replacements or enhancers for ITO/FTO electrodes, as graphene doping is compatible with both FTO and ITO substrates [56].

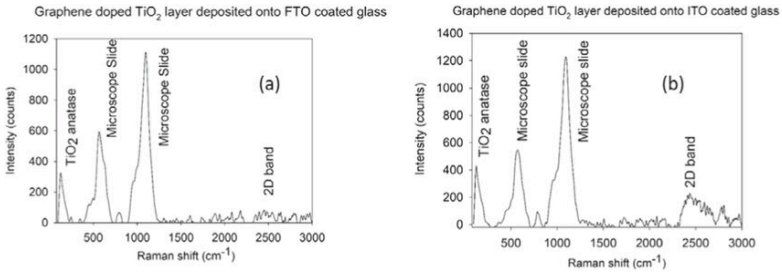


Figure 9. Graphene improves the electrical performance of TiO_2 layers on both FTO and ITO substrates [56]

As a result of these upgrades, the electrical resistance of graphene will be lowered and it will be more similar to conventional transparent conductive oxides (TCOs) in terms of electrical properties but still graphene will have better ductility. Compared to TCO electrodes, graphene has the advantage of being of atomic-level thickness which makes it possible to fabricate extremely flexible PSC structures that retain their performance even after 10K bending cycles [57].

DOI: 10.54254/2753-8818/2026.LA30799

4.2.2. Photomechanical protection

Graphene can also protect perovskite films from environmental stress. During fabrication, ultrasonication often reduces graphene's conductivity, but when properly processed, a single graphene sheet can act as a strong physical barrier against moisture and oxygen penetration.

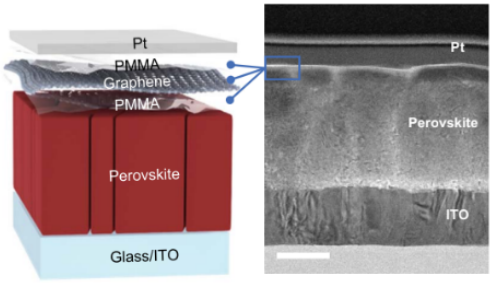


Figure 10. Device structure and the corresponding cross-sectional TEM image of a perovskite device slice fabricated by focused ion beam [58]

A single graphene layer deposited on the perovskite film is capable of impeding the entry of water vapor and oxygen molecules and thus photodegradation and halide volatilization can be limited. Moreover, due to its high permeability and good thermal conductivity, it can shield the active layer from environmental and mechanical stress. Li et al. [58] showed that graphene layers coupled with PMMA can physically interact with the perovskite lattice, thereby increasing the lattice's flexibility and thermal stability. In addition, the graphene-polymer composite can still hold more than 95% of its initial PCE after thousands of hours of continuous illumination, which means that we are one step closer to long-term stable and flexible PSCs.

4.3. Current challenges and potentials

Graphene-based PSCs have performed remarkably well, but there are several more challenges to deal with. First, scalable manufacturing remains problematic. Most graphene additions have been demonstrated in small-area devices, while large-area fabrication can introduce cracks due to the complex lamination process, leading to uneven conductivity [4]. Second, increasing the thickness of the graphene layer improves conductivity but generally reduces optical transmittance. Even small losses in transmittance can reduce the current density and fill factor of the device [59]. Third, although graphene derivatives can passivate defects, their work function and dipole interactions with transport layers (e.g., SnO_2 or self-assembled monolayer-based contacts) are tuned empirically rather than predictively. The durability of graphene-polymer composites has been greatly improved[58], but large-scale testing under thermal cycling conditions still requires further improvement.

5. Knowledge gaps and future perspectives for graphene-based PSCs

Despite strong progress, graphene-based perovskite solar cells still face several technical and practical barriers that limit industrial application. Most high efficiencies are achieved only on small laboratory samples. When devices are scaled up, wet transfers and laminations often introduce wrinkles, cracks, and residues, creating uneven resistance and instability during drying or annealing. A transfer-free or defect-tolerant process that fits blade, slot-die, or hybrid vacuum coating lines is still missing, and future work should focus on inline monitoring and uniform film formation

DOI: 10.54254/2753-8818/2026.LA30799

[14,15,17,18]. Lowering sheet resistance through multilayer stacking or doping usually sacrifices optical transmittance and durability. Since present perovskites already perform close to their theoretical limit, even slight optical losses reduce current and fill factor. Stable, transparent, and conductive oxide–graphene or polymer–graphene hybrids must be developed and tested under identical long-term conditions [2,4,56,59]. Graphene derivatives such as GO, rGO, and GQDs can passivate defects and improve extraction, but their interfacial energy alignment with SnO_2, C_{60}, and SAM layers remains empirical. A quantitative link between graphene surface chemistry, interfacial dipoles, and non-radiative voltage loss is still lacking. Combining UPS, KPFM, and ToF-SIMS with electroluminescence and device modeling may allow prediction and design of energy levels [3,8,32,35]. Although graphene reduces current–voltage hysteresis, the mechanism is unclear. Its effects on ion mobility and electric-field screening have not been fully modeled. A drift–diffusion framework that accounts for graphene's position in ETL, HTL, or bulk layers, and that correlates experimental hysteresis and impedance data, could explain its stabilizing role [29,38,39,40]. Reliability and sustainability also remain open challenges. Few studies report full ISOS testing, thermal cycling, or bending fatigue, and encapsulation compatibility has not been benchmarked. Long-term viability will require standardized stress protocols, life-cycle and economic analyses, and comparison of graphene routes such as CVD and wet reduction with conventional ITO or FTO systems [1,10,24,26].

6. Conclusion

Due to the chemical properties of the transport layer material, which is susceptible to interacting with the environment, and its fragile physical properties, early PSCs could not withstand prolonged sunlight, high temperatures, or bending. Adding graphene derivatives made the film more stable and achieved higher photoelectric conversion efficiency. Devices modified with graphene now achieve higher power conversion efficiency, longer carrier lifetimes, and better operational stability than conventional designs. Yet, commercialization remains a challenge due to difficulties in mass production, for instance, high production costs and transfer defects. Subsequent investigations are expected to focus on the development of easier and more scalable production methods and attaining more precise control of the graphene-perovskite interface. By working on these issues, the graphene-based perovskite solar cells can become a reality beyond the lab and a significant part of the renewable energy of the future.

References

[1] P. T. Mokabane, V. T. Lukong, and T.-C. Jen, "A review of the effect of stability issues and wide-bandgap in the application of perovskite solar cells, " Mater. Renew. Sustain. Energy, vol. 14, no. 2, p. 34, Aug. 2025, doi: 10.1007/s40243-025-00307-9.

[2] H. Luo, X. Lin, X. Hou, L. Pan, S. Huang, and X. Chen, "Efficient and Air-Stable Planar Perovskite Solar Cells Formed on Graphene-Oxide-Modified PEDOT: PSS Hole Transport Layer, " Nano-Micro Lett., vol. 9, no. 4, p. 39, Oct. 2017, doi: 10.1007/s40820-017-0140-x.

[3] Y. Rui et al., "Defect passivation and electrical conductivity enhancement in perovskite solar cells using functionalized graphene quantum dots, " Mater. Futur., vol. 1, no. 4, p. 045101, Dec. 2022, doi: 10.1088/2752-5724/ac9707.

[4] F. Znidi, M. Morsy, and Md. Nizam Uddin, "Recent advances of graphene-based materials in planar perovskite solar cells, " Nanotechnol., vol. 5, p. 100061, 2024, doi: 10.1016/j.nxnano.2024.100061.

[5] R. Vanaraj, V. Murugesan, and B. Rathinam, "The Role of Optimal Electron Transfer Layers for Highly Efficient Perovskite Solar Cells—A Systematic Review, " Micromachines, vol. 15, no. 7, p. 859, July 2024, doi: 10.3390/mi15070859.

DOI: 10.54254/2753-8818/2026.LA30799

[6] F. M. Rombach, S. A. Haque, and T. J. Macdonald, "Lessons learned from spiro-OMeTAD and PTAA in perovskite solar cells, " Oct. 2021, doi: 10.1039/D1EE02095A.
[7] H. Zhang and N.-G. Park, "Progress and issues in p-i-n type perovskite solar cells, " DeCarbon, vol. 3, p. 100025, Mar. 2024, doi: 10.1016/j.decarb.2023.100025.
[8] Z. Yi et al., "Self-assembled monolayers (SAMs) in inverted perovskite solar cells and their tandem photovoltaics application, " Interdiscip. Mater., vol. 3, no. 2, pp. 203–244, 2024, doi: 10.1002/idm2.12145.
[9] W. Fu et al., "Self-assembled monolayers for perovskite solar cells, " Rev. Mater. Res., vol. 1, no. 1, p. 100017, Jan. 2025, doi: 10.1016/j.revmat.2025.100017.
[10] P. Chen et al., "The Promise and Challenges of Inverted Perovskite Solar Cells, " Chem. Rev., vol. 124, no. 19, pp. 10623–10700, Oct. 2024, doi: 10.1021/acs.chemrev.4c00073.
[11] X. Zheng et al., "Solvent engineering for scalable fabrication of perovskite/silicon tandem solar cells in air, " Nat. Commun., vol. 15, no. 1, p. 4907, June 2024, doi: 10.1038/s41467-024-49351-5.
[12] M. Chen et al., "Low-temperature sequential deposition for efficient inverted perovskite solar cells, " Nat. Commun., vol. 16, no. 1, p. 5746, July 2025, doi: 10.1038/s41467-025-61144-y.
[13] Y. Yang et al., "Green anti-solvent engineering for high-efficiency and environmentally friendly perovskite solar cells, " RSC Adv., vol. 14, no. 44, pp. 32370–32388, Oct. 2024, doi: 10.1039/D4RA05082G.
[14] V. C. M. Duarte and L. Andrade, "Recent Advancements on Slot-Die Coating of Perovskite Solar Cells: The Lab-to-Fab Optimisation Process, " Energies, vol. 17, no. 16, p. 3896, Jan. 2024, doi: 10.3390/en17163896.
[15] E. Parvazian and T. Watson, "The roll-to-roll revolution to tackle the industrial leap for perovskite solar cells, " Nat. Commun., vol. 15, no. 1, p. 3983, May 2024, doi: 10.1038/s41467-024-48518-4.
[16] W. Yang et al., "Unlocking Voltage Potentials of Mixed-Halide Perovskite Solar Cells via Phase Segregation Suppression, " Adv. Funct. Mater., vol. 32, no. 12, p. 2110698, 2022, doi: 10.1002/adfm.202110698.
[17] H. C. Weerasinghe et al., "The first demonstration of entirely roll-to-roll fabricated perovskite solar cell modules under ambient room conditions, " Nat. Commun., vol. 15, no. 1, p. 1656, Mar. 2024, doi: 10.1038/s41467-024-46016-1.
[18] M. Yao et al., "Minimizing Performance Loss in Blade-Coated Large-Area Perovskite Solar Cells Via Semi-Sealed Gas Quenching, " Adv. Funct. Mater., vol. 35, no. 16, p. 2418915, 2025, doi: 10.1002/adfm.202418915.
[19] S. Qiu et al., "Over one-micron-thick void-free perovskite layers enable highly efficient and fully printed solar cells, " Energy Environ. Sci., vol. 18, no. 12, pp. 5926–5939, June 2025, doi: 10.1039/D5EE01722J.
[20] H. Li et al., "Sequential vacuum-evaporated perovskite solar cells with more than 24% efficiency, " Sci. Adv., vol. 8, no. 28, p. eabo7422, July 2022, doi: 10.1126/sciadv.abo7422.
[21] Y. Fan et al., "An efficient and precise solution-vacuum hybrid batch fabrication of 2D/3D perovskite submodules, " Nat. Commun., vol. 16, no. 1, p. 7019, July 2025, doi: 10.1038/s41467-025-62392-8.
[22] Z. Kalantari Bolaghi, C. Rodriguez-Seco, A. Yurtsever, and D. Ma, "Exploring the Remarkably High Photocatalytic Efficiency of Ultra-Thin Porous Graphitic Carbon Nitride Nanosheets, " Nanomaterials, vol. 14, no. 1, p. 103, Jan. 2024, doi: 10.3390/nano14010103.
[23] V. L. Vilesh, N. Santha, and G. Subodh, "Influence of Li2MoO4 and polytetrafluoroethylene addition on the cold sintering process and dielectric properties of BaBiLiTeO6 ceramics, " Ceram. Int., vol. 47, no. 21, pp. 30756–30763, Nov. 2021, doi: 10.1016/j.ceramint.2021.07.255.
[24] Y. Guo et al., "Efficient inverted perovskite solar cells with a low-temperature processed NiOx/SAM hole transport layer, " J. Mater. Chem. C, vol. 12, no. 4, pp. 1507–1515, Jan. 2024, doi: 10.1039/D3TC03575A.
[25] H. Tang et al., "Reinforcing self-assembly of hole transport molecules for stable inverted perovskite solar cells, " Science, vol. 383, no. 6688, pp. 1236–1240, Mar. 2024, doi: 10.1126/science.adj9602.
[26] X. Lin et al., "In situ growth of graphene on both sides of a Cu–Ni alloy electrode for perovskite solar cells with improved stability, " Nat. Energy, vol. 7, no. 6, pp. 520–527, June 2022, doi: 10.1038/s41560-022-01038-1.
[27] J. Xue, "Secure the electrodes, " Nat. Energy, vol. 7, no. 6, pp. 476–477, June 2022, doi: 10.1038/s41560-022-01040-7.
[28] S. V. Oleĭnik and O. N. Chugaĭ, "Thermal depolarization of naturally polarized zinc selenide polycrystals, " Tech. Phys. Lett., vol. 32, no. 8, pp. 716–718, Aug. 2006, doi: 10.1134/S1063785006080232.
[29] A. Singh and A. Gagliardi, "Drift-diffusion modeling of perovskite solar cells: past and future possibilities, " EES Sol., vol. 1, no. 5, pp. 694–711, Oct. 2025, doi: 10.1039/D5EL00040H.
[30] S. Xiong et al., "Reducing nonradiative recombination for highly efficient inverted perovskite solar cells via a synergistic bimolecular interface, " Nat. Commun., vol. 15, no. 1, p. 5607, July 2024, doi: 10.1038/s41467-024-50019-3.
[31] "Improved charge extraction in inverted perovskite solar cells with dual-site-binding ligands | Science." Accessed: Oct. 25, 2025. [Online]. Available: https: //www.science.org/doi/10.1126/science.adm9474

DOI: 10.54254/2753-8818/2026.LA30799

[32] Y. Zheng et al., "Towards 26% efficiency in inverted perovskite solar cells via interfacial flipped band bending and suppressed deep-level traps, " Energy Environ. Sci., vol. 17, no. 3, pp. 1153–1162, Feb. 2024, doi: 10.1039/D3EE03435F.
[33] G. J. W. Aalbers, T. P. A. van der Pol, K. Datta, W. H. M. Remmerswaal, M. M. Wienk, and R. A. J. Janssen, "Effect of sub-bandgap defects on radiative and non-radiative open-circuit voltage losses in perovskite solar cells, " Nat. Commun., vol. 15, no. 1, p. 1276, Feb. 2024, doi: 10.1038/s41467-024-45512-8.
[34] X. He et al., "Suppressing surface and interface recombination to afford efficient and stable inverted perovskite solar cells, " Nanoscale, vol. 16, no. 36, pp. 17042–17048, Sept. 2024, doi: 10.1039/D4NR02391A.
[35] J. Xia, M. Sohail, and M. K. Nazeeruddin, "Efficient and Stable Perovskite Solar Cells by Tailoring of Interfaces, " Adv. Mater., vol. 35, no. 31, p. 2211324, 2023, doi: 10.1002/adma.202211324.
[36] D. Lan, "The physics of ion migration in perovskite solar cells: Insights into hysteresis, device performance, and characterization, " Prog. Photovolt. Res. Appl., vol. 28, no. 6, pp. 533–537, 2020, doi: 10.1002/pip.3203.
[37] "Hysteresis and Its Correlation to Ionic Defects in Perovskite Solar Cells | The Journal of Physical Chemistry Letters." Accessed: Oct. 25, 2025. [Online]. Available: https: //pubs.acs.org/doi/10.1021/acs.jpclett.3c03146
[38] Z. S. Wang et al., "Device deficiency and degradation diagnosis model of Perovskite solar cells through hysteresis analysis, " Nat. Commun., vol. 15, no. 1, p. 9647, Nov. 2024, doi: 10.1038/s41467-024-53162-z.
[39] J. Thiesbrummel et al., "Ion-induced field screening as a dominant factor in perovskite solar cell operational stability, " Nat. Energy, vol. 9, no. 6, pp. 664–676, June 2024, doi: 10.1038/s41560-024-01487-w.
[40] T. Kim et al., "Mapping the pathways of photo-induced ion migration in organic-inorganic hybrid halide perovskites, " Nat. Commun., vol. 14, no. 1, p. 1846, Apr. 2023, doi: 10.1038/s41467-023-37486-w.
[41] Z. Zhang et al., "Suppression of phase segregation in wide-bandgap perovskites with thiocyanate ions for perovskite/organic tandems with 25.06% efficiency, " Nat. Energy, vol. 9, no. 5, pp. 592–601, May 2024, doi: 10.1038/s41560-024-01491-0.
[42] K. Datta et al., "Local halide heterogeneity drives surface wrinkling in mixed-halide wide-bandgap perovskites, " Nat. Commun., vol. 16, no. 1, p. 1967, Feb. 2025, doi: 10.1038/s41467-025-57010-6.
[43] Q. Ma et al., "One-step dual-additive passivated wide-bandgap perovskites to realize 44.72%-efficient indoor photovoltaics, " Energy Environ. Sci., vol. 17, no. 5, pp. 1637–1644, Mar. 2024, doi: 10.1039/D3EE04022D.
[44] X. Ji et al., "Correlating halide segregation of wide-bandgap perovskites with the methoxy group in organic hole-selective materials, " Chem. Sci., vol. 16, no. 19, pp. 8569–8576, May 2025, doi: 10.1039/D4SC08810G.
[45] X. Ji et al., "Efficient wide-bandgap perovskite solar cells with open-circuit voltage deficit below 0.4 V via hole-selective interface engineering, " Sci. China Chem., vol. 67, no. 6, pp. 2102–2110, June 2024, doi: 10.1007/s11426-023-1966-1.
[46] J. Heo et al., "High Open-Circuit Voltage Wide-Bandgap Perovskite Solar Cell with Interface Dipole Layer, " Small, vol. 20, no. 50, p. 2404784, 2024, doi: 10.1002/smll.202404784.
[47] "Highest Perovskite Solar Cell Efficiencies (2025 Update), " Fluxim. Accessed: Oct. 25, 2025. [Online]. Available: https: //www.fluxim.com/research-blogs/perovskite-silicon-tandem-pv-record-updates
[48] Y. Wang, J. Hüpkes, S. Ravishankar, B. Klingebiel, and T. Kirchartz, "Loss Analysis of Halide-Perovskite Solar Cells Deposited on Textured Substrates, " Sol. RRL, vol. 9, no. 7, p. 2400829, 2025, doi: 10.1002/solr.202400829.
[49] "Highly Efficient and Scalable p-i-n Perovskite Solar Cells Enabled by Poly-metallocene Interfaces | Journal of the American Chemical Society." Accessed: Oct. 25, 2025. [Online]. Available: https: //pubs.acs.org/doi/10.1021/jacs.4c02220
[50] Y. Yuan, G. Yan, S. Akel, U. Rau, and T. Kirchartz, "Deriving mobility-lifetime products in halide perovskite films from spectrally- and time-resolved photoluminescence, " Nov. 04, 2024, arXiv: arXiv: 2411.01912. doi: 10.48550/arXiv.2411.01912.
[51] M. C. Gélvez-Rueda, N. Renaud, and F. C. Grozema, "Temperature Dependent Charge Carrier Dynamics in Formamidinium Lead Iodide Perovskite, " J. Phys. Chem. C, vol. 121, no. 42, pp. 23392–23397, Oct. 2017, doi: 10.1021/acs.jpcc.7b09303.
[52] P. Shi et al., "Strain regulates the photovoltaic performance of thick-film perovskites, " Nat. Commun., vol. 15, no. 1, p. 2579, Mar. 2024, doi: 10.1038/s41467-024-47019-8.
[53] Y. S. Shin et al., "Damp-heat stable and efficient perovskite solar cells and mini-modules with a tBP-free hole-transporting layer, " Energy Environ. Sci., vol. 18, no. 7, pp. 3269–3277, Apr. 2025, doi: 10.1039/D4EE05699J.
[54] H. Zhou et al., "Efficient and stable perovskite mini-module via high-quality homogeneous perovskite crystallization and improved interconnect, " Nat. Commun., vol. 15, no. 1, p. 6679, Aug. 2024, doi: 10.1038/s41467-024-50962-1.
[55] X. Zhang et al., "Graphene oxide as an additive to improve perovskite film crystallization and morphology for high-efficiency solar cells, " RSC Adv., vol. 8, no. 2, pp. 987–993, 2018, doi: 10.1039/C7RA12049D.

DOI: 10.54254/2753-8818/2026.LA30799

[56] S. Pat et al., "Electrochromic Properties of Graphene Doped TiO_2 Layer Deposited by Thermionic Vacuum Arc, " ECS J. Solid State Sci. Technol., vol. 9, no. 6, p. 061016, July 2020, doi: 10.1149/2162-8777/aba728.
[57] T. Wang et al., "Recent Developments in Flexible Transparent Electrode, " Crystals, vol. 11, no. 5, p. 511, May 2021, doi: 10.3390/cryst11050511.
[58] Q. Li et al., "Graphene-polymer reinforcement of perovskite lattices for durable solar cells, " Science, vol. 387, no. 6738, pp. 1069–1077, Mar. 2025, doi: 10.1126/science.adu5563.
[59] Y. S. Woo, "Transparent Conductive Electrodes Based on Graphene-Related Materials, " Micromachines, vol. 10, no. 1, p. 13, Dec. 2018, doi: 10.3390/mi10010013.